Superfluid Vortex Front at $T \rightarrow 0$: Decoupling from the Reference Frame

J. J. Hosio,[1] V. B. Eltsov,[1] R. de Graaf,[1] P. J. Heikkinen,[1] R. Hänninen,[1] M. Krusius,[1] V. S. L'vov,[2] and G. E. Volovik[1,3]

[1]*Low Temperature Laboratory, School of Science, Aalto University, FI-00076 AALTO, Finland*
[2]*Department of Chemical Physics, The Weizmann Institute of Science, Rehovot 76100, Israel*
[3]*Landau Institute for Theoretical Physics, Kosygina 2, 119334 Moscow, Russia*
(Received 20 June 2011; published 21 September 2011)

Steady-state turbulent motion is created in superfluid ^{3}He-B at low temperatures in the form of a turbulent vortex front, which moves axially along a rotating cylindrical container of ^{3}He-B and replaces vortex-free flow with vortex lines at constant density. We present the first measurements on the thermal signal from dissipation as a function of time, recorded at $0.2T_c$ during the front motion, which is monitored using NMR techniques. Both the measurements and the numerical calculations of the vortex dynamics show that at low temperatures the density of the propagating vortices falls well below the equilibrium value, i.e., the superfluid rotates at a smaller angular velocity than the container. This is the first evidence for the decoupling of the superfluid from the container reference frame in the zero-temperature limit.

Introduction.—For 80 years the phenomenological two-fluid model of Tisza and Landau has been the starting point for discussions on dynamics in superfluids. Onsager and Feynman introduced the quantized vortex, which plays an all important role in the dynamics: Vortices mediate the interaction between the superfluid and normal components of the liquid via reactive and dissipative friction forces [1]. Vortices also allow the superfluid component to participate in nonpotential flow and thus in rotation.

In a container which rotates at constant angular velocity Ω, a viscous liquid always finally relaxes to the equilibrium state—the state of solid-body rotation with the container. Superfluid rotation displays more variation: It is generally assumed that at $T = 0$, where the normal component is absent, a vortex-free superfluid remains at rest in the laboratory frame, when its container is set into rotation. However, vortices change the situation, by acquiring an array of rectilinear vortex lines the superfluid component is also able to participate in rotational flow and to mimic solid-body rotation. At finite temperature the mutual friction force between vortices and the normal component provides the coupling between the container frame and that of the rotating superfluid, so that in complete equilibrium these frames coincide—vortices are at rest in the container frame. However, the coupling between the frames decreases with decreasing temperature, and is lost in the $T \rightarrow 0$ limit when the normal component vanishes. Here we discuss an experimental example of the decoupling of the frames—the propagating vortex front in superfluid ^{3}He-B. We find that in the low-T limit, the superfluid component behind the front develops its own rotating reference frame, whose angular velocity is smaller than that of the container and is decreasing with decreasing coupling.

Turbulent vortex-front motion is ubiquitous in the dynamics of both viscous fluids [2] and superfluids [3].

In superfluid ^{4}He turbulent fronts and plugs are known from pipe flow driven by thermal counter currents of the normal and superfluid components. In a long cylinder of superfluid ^{3}He-B the spin-up response of the superfluid component from rest to rotation often takes place as an axially propagating precessing vortex front [4]. The motion of the front is launched after a sudden localized turbulent burst. This can be engineered to happen at constant angular velocity Ω, if the superfluid is initially in the metastable vortex-free Landau state and the turbulent burst is triggered externally. Once formed, the front consists of a turbulent core, with an axial length comparable to the cylinder radius R, and a quasilaminar tail in the form of a helically twisted bundle [5] of vortex lines. The front is one of the few examples of steady-state turbulent motion in superfluids, which are presently available for experimental investigations in the $T \rightarrow 0$ limit. We have performed the first direct measurement of the heat released by such quantum-turbulent motion [6].

The difference in the free energy of the vortex-free superfluid and that in equilibrium rotation is $\pi \rho_s R^4 \Omega^2/4$ per unit length of the cylinder of radius R. Here ρ_s is the density of the superfluid component and a small correction from the discrete nature of vortices is neglected. In our measurements the spin-up process happens at $\Omega = \text{const}$ while the normal component is corotating with the container. In this case the work performed by the rotation drive can be found using the balance of angular momentum transfer. It can then be shown that the heat, expected to be generated in the spin-up process, is equal to the change of the energy of the superfluid [7].

The simplest model of stationary-state front motion is that of a thin turbulent front to which all dissipation is concentrated and where the laminar relaxation to rectilinear vortex lines behind the front is neglected. If the front moves with the velocity V, the dissipation rate is

$$\dot{Q} = \frac{\pi \rho_s}{4} R^4 \Omega^2 V. \qquad (1)$$

For stationary-state motion Eq. (1) gives the maximum possible rate of heat release. As found in Ref. [4], with decreasing temperature the front velocity reflects the properties of the different regimes of superfluid vortex flow and at about $0.25 T_c$ it settles down on a plateau which was found to be given by $V \approx \alpha_{\rm eff} \Omega R$, where $\alpha_{\rm eff} \sim 0.1$ is a constant, generated by the turbulence in the front. In this case the signal intensity is $\dot{Q} \propto \Omega^3$ with only weak temperature dependence.

Experimental techniques.—In Fig. 1 the ^{3}He-B sample in the top section of the long sample cylinder can be organized to rotate around its symmetry axis at constant angular velocity Ω in the vortex-free state [8]. Here the superfluid fraction is at rest in the laboratory frame ($\mathbf{v}_s = \mathbf{0}$), while the normal excitations are in solid-body rotation ($\mathbf{v}_n = \mathbf{\Omega} \times \mathbf{r}$). The distribution of vortices and superfluid counterflow as well as the motion of vortices is surveyed with two NMR detector coils [9]. To trigger the front propagation, we use the Kelvin-Helmholtz shear flow instability of the A-B interface [10]. The instability occurs at a well-defined critical velocity $\Omega_{\rm AB}$, which depends on the magnetic stabilization field H_b and its gradient at the location of the A-B interface. In our thermal measurements $\Omega_{\rm AB}$ is traversed by sweeping H_b at $\Omega = {\rm const}$, for example, by increasing H_b from zero until the A phase is formed. The important consequence from the instability event is the escape of a number of vortex loops across the A-B interface from the A to the B phase side. The loops interact and produce a large number of vortices in a turbulent burst close to the A-B interface. In the setup of Fig. 1 the instability occurs simultaneously at the two A-B interfaces. Thus both upward and downward propagating fronts are set into motion. These come to a halt when the fronts reach the top and bottom end plates of the sample cylinder. The final state, after all transients have decayed, is the equilibrium vortex state with an array of rectilinear vortex lines, as can be verified with NMR measurements [11]. However, how is the equilibrium state reached?

Thermal measurements.—The heat released in the spin-up process is recorded as a temperature rise across the lower orifice, which is the dominant thermal resistance in the ballistic regime. The value of this resistance is calibrated from the temperature increase as a function of the known heating power, using one quartz tuning fork oscillator as thermometer and the other as heater [12]. The calibration also gives a residual heat leak to the ^{3}He sample of 15 pW at $\Omega = 0$, which increases by ~ 4 pW for a 1 rad/s increment in Ω.

Examples of the thermal measurements of the front propagation are shown in Fig. 2. The total energy release, integrated above background, matches the expectations: 0.55 and 0.75 nJ at 1 and 1.2 rad/s, respectively, versus the expected values of 0.73 and 1.01 nJ. The difference of 25% between the measured and expected heat release can be ascribed to uncertainties in the bolometer calibration.

The arrival of the front to the end of the sample, as determined from the NMR measurements, corresponds to the maximum of the power signal, while most of the energy is released only after this moment. Thus by the time the front has reached the end of the sample, the vortex configuration behind the front still includes less vortices than
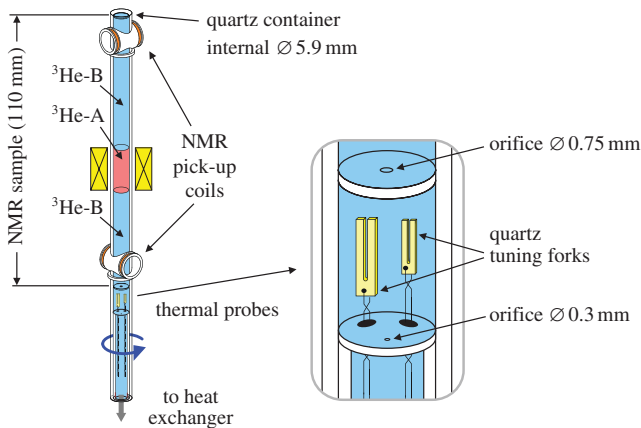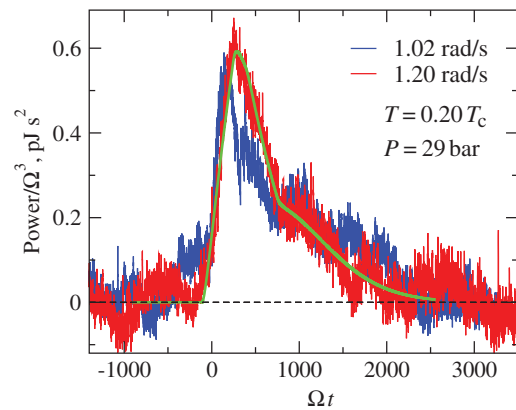

FIG. 1 (color). Measuring setup. Two independent cw NMR spectrometers are used to monitor vortex-front motion in the sample container above the $\varnothing$ 0.75 mm orifice. The middle section with the quartz tuning fork oscillators is employed for thermometry and quasiparticle bolometry. The bottom section below the $\varnothing$ 0.3 mm orifice provides the thermal contact to the refrigerator. The superconducting solenoid in the center of the NMR sample produces the H_b field for stabilizing the ^{3}He-A phase. This A-phase barrier layer divides the NMR sample in two ^{3}He-B sections of equal length.

FIG. 2 (color). Two Ω-scaled bolometer signals. Time $t = 0$ is assigned to the moment when the trigger signal (cooling due to the latent heat in B to A transition) is observed. This trigger signal and the background heat leak have been removed by subtracting the equivalent signal measured in the equilibrium vortex state. The green curve represents a fit to the experimental record at $\Omega = 1.2$ rad/s. The thermal time constant of the bolometer is about 25 s, which is much shorter than the time scale of front propagation.

in the equilibrium state. The shoulder at $\Omega t \sim 1000$ and the duration of the signal hint that the late relaxation behind the front is the laminar spin-up of the superfluid component [13]. The fit of the experimental record at 1.2 rad/s to a simple model which accounts for the turbulent front creating 0.35 of the equilibrium number of vortices, followed by laminar relaxation with a time constant of 500 s, is shown by the green curve in Fig. 2 and is in reasonable agreement with the measurement. Thus a consistent overall interpretation of the thermal measurements inevitably requires that during the axial front propagation the number of vortices is much reduced from that in equilibrium rotation.

Precessing vortex motion.—Independent confirmation of the low density of vortices behind the front comes from observations of precessing vortex motion around the axis of the cylinder, Fig. 3. The precession is visible as oscillations of the NMR signal when the vortex arrangement is not perfectly axially symmetric, which often happens in the front and immediately behind it. For vortex clusters with uniform density the ratio of their precession frequency Ω_s to Ω is equal to the ratio of the number of vortices in the cluster to that in the equilibrium state. For the front itself the precession frequency is about half of Ω_s [5]. Thus the measurement in Fig. 3 shows that at $0.2T_c$ the cluster behind the front has about 0.4 of the equilibrium vortex density, in agreement with the thermal signal.

Numerical calculations.—To understand the observed reduction in the number of vortices, numerical simulations have been performed using the vortex filament model and the Biot-Savart law for computing $\mathbf{v}_s$ [11]. Above $0.3T_c$,

such simulations demonstrate that the average vortex number per cross section stays constant as a function of z behind the front and corresponds to solid-body rotation with the angular velocity Ω of the container [11]. Below $0.3T_c$, the vortex density behind the front also stays constant as a function of z, but corresponds to solid-body rotation with a velocity $\Omega_s < \Omega$ (Fig. 4). In other words, the vortex system develops its own rotating frame. The velocity of the vortex frame Ω_s decreases prominently with decreasing temperature and at $0.20T_c$ agrees with the experimentally determined value of about 0.4Ω. Ω_s is found to depend weakly on the initial conditions, i.e., on the number and configuration of the seed vortices which start the front motion. A similar dependence is observed also experimentally. The calculations confirm that the precession frequency of the front is approximately $\Omega_s/2$ (insert in Fig. 4). The difference in the rotation velocities of the front and the vortex bundle behind it is made possible by vortex reconnections, as seen in the lower panel of Fig. 4. These reconnections lead to the steady-state turbulence in the front.
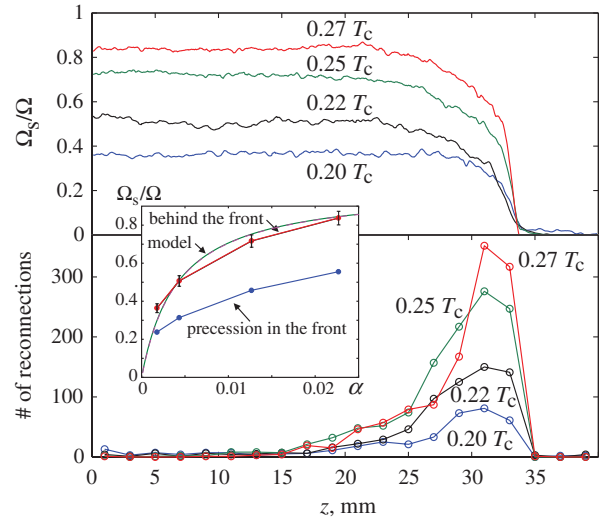
FIG. 4 (color). Vortex front in numerical calculations. Snapshots of vortex configurations at different temperatures are analyzed when the front is located at the same axial position $z = 34$ mm. Top: Azimuthal velocity $\langle v_s \rangle_\phi = \Omega_s r$ as a function of z, when averaged over the vortices in the cross section $0 \leq r \leq 0.8R$. The vortex-free state is before the front ($z > 35$ mm) and the quasiequilibrium vortex state with $\Omega_s(T) < \Omega$ is behind the front. Inset: The precession frequency of the vortex ends in the front region ($z \gtrsim 29$ mm), value of Ω_s averaged over z behind the front, and the interpolation formula Eq. (6) plotted as a function of the mutual friction parameter $\alpha(T)$. The uncertainty bars denote the z-averaged 95% confidence limit. Bottom: Turbulence in the front is supported by vortex reconnections, which have been counted here within bins of width $\Delta z = 2$ mm over a time interval in which the front propagates 0.5 mm. Parameters: cylinder length 40 mm, $R = 1.5$ mm, $\Omega = 1.0$ rad/s, $\alpha(T) = 33.2 \exp(-1.97T_c/T)$.
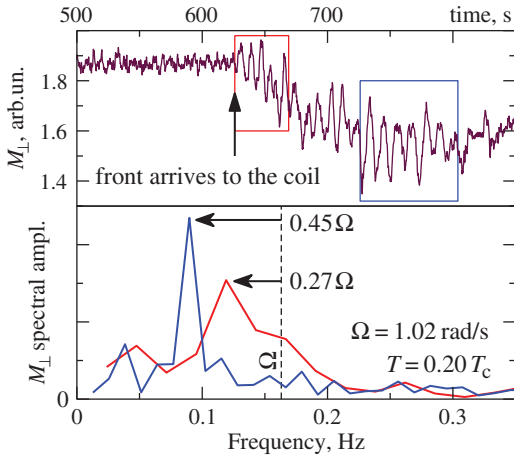

FIG. 3 (color). Precessing motion in the vortex front and the vortex bundle behind it. Top: Oscillations start in the NMR signal (total transverse magnetization $M_\perp$ [17]) when the front arrives at the pick-up coil. Their source is the precessing motion of vortices. Bottom: Fourier transforms of parts of the NMR signal marked in the top panel: The front (red line) and the cluster behind it (blue line). Since the NMR coil is fixed to the rotating frame, the precession frequencies in the laboratory frame are counted from the angular velocity Ω, as shown by the arrows.

Decoupling of rotating frames.—The emergence of a new rotating frame with angular velocity Ω_s can be qualitatively understood on the basis of the coarse-grained hydrodynamic equation for $\mathbf{v}_s$,

$$\frac{\partial \mathbf{v}_s}{\partial t} + \nabla\mu - \mathbf{v}_s \times (\nabla \times \mathbf{v}_s) = \mathbf{F}_\alpha + \mathbf{F}_\lambda. \qquad (2)$$

Unlike classical fluids, two forces appear here on the right-hand side: the mutual friction force between the normal and superfluid components,

$$\mathbf{F}_\alpha = -\alpha\hat{\omega} \times [(\mathbf{v}_s - \mathbf{v}_n) \times (\nabla \times \mathbf{v}_s)], \qquad (3)$$

and the force due to the line tension [14],

$$\mathbf{F}_\lambda = -\lambda(\nabla \times \mathbf{v}_s) \times (\nabla \times \hat{\omega}). \qquad (4)$$

Here $\hat{\omega}$ is a unit vector along the vorticity $\nabla \times \mathbf{v}_s$, α is the dissipative mutual friction parameter (while the reactive mutual friction force with the parameter α' is neglected at low T). The line tension parameter λ is given by $\lambda = (\kappa/4\pi)\ln(\ell/a)$, where κ is the circulation quantum, a is the vortex core diameter, and ℓ the intervortex distance. Two different Reynolds numbers, Re_α and Re_λ, are needed to characterize superfluid vortex flow at the fixed normal component. These parameters represent the relative magnitude of the inertial term in Eq. (1) with respect to the mutual friction ($\mathbf{F}_\alpha$) and line tension ($\mathbf{F}_\lambda$) forces:

$$\mathrm{Re}_\alpha \approx 1/\alpha, \qquad \mathrm{Re}_\lambda = UR/\lambda = \Omega R^2/\lambda. \qquad (5)$$

The two Reynolds numbers control different regimes of the two fluid hydrodynamics: for turbulent flow one requires $\mathrm{Re}_\lambda \gg 1$ and $\mathrm{Re}_\alpha \gtrsim 1$, while quasiclassical Kolmogorov turbulence is found in the regime $\mathrm{Re}_\alpha < (\mathrm{Re}_\lambda)^{1/2}$ and the nonstructured quantum turbulence in the Vinen regime $\mathrm{Re}_\alpha > (\mathrm{Re}_\lambda)^{1/2}$ [9].

The Reynolds numbers describe the two competing tendencies experienced by the vortices behind the front: spin-up due to mutual friction from the normal component, and spin-down by the precessing vortex front, which rotates slower than the vortex bundle behind the front. The interplay of these mechanisms leads to the establishment of a quasiequilibrium vortex state behind the front. This state is in solid-body rotation with the velocity Ω_s, which is in general a function of the two Reynolds numbers, changing from the full coupling ($\Omega_s = \Omega$) at high temperatures to the decoupled state ($\Omega_s \rightarrow 0$) in the $T \rightarrow 0$ limit. As a simple interpolation between these two regimes we may suggest

$$\Omega_s/\Omega = (1 + \mathrm{Re}_\alpha/\mathrm{Re}_\lambda)^{-1}, \qquad (6)$$

which is in agreement with the results of the numerical simulations (Fig. 4, insert).

Conclusions.—Both measurements and numerical calculations demonstrate that the vortex state behind the propagating vortex front corresponds to quasiequilibrium solid-body rotation at a velocity Ω_s which is less than the angular velocity of the normal component: $\Omega_s < \Omega$. Thus the angular velocity of the frame in which the vortices are at rest deviates from that of the container. The decoupling of the two frames becomes more and more prominent below the characteristic temperature of $0.3T_c$, owing to the competing influences from mutual friction and vortex line tension. This leads to a total decoupling in the limit $T \rightarrow 0$, unless a new effect intervenes. Possible candidates for such zero-temperature coupling include the circular-motion analog of the Unruh effect [15] and the interaction of the vortex-core-bound quasiparticle excitations [16] with the container boundaries.

[1] G. E. Volovik, *The Universe in a Helium Droplet* (Clarendon Press, Oxford, 2003).
[2] See, e.g., G. Ahlers and D. S. Cannell, Phys. Rev. Lett. **50**, 1583 (1983); J. Fineberg and V. Steinberg, *ibid.* **58**, 1332 (1987); B. Hof, A. Juel, and T. Mullin, *ibid.* **91**, 244502 (2003).
[3] See, e.g., R. P. Slegtenhorst *et al.*, Physica (Amsterdam) **113B**, 367 (1982); and references therein.
[4] V. B. Eltsov *et al.*, Phys. Rev. Lett. **99**, 265301 (2007).
[5] V. B. Eltsov *et al.*, Phys. Rev. Lett. **96**, 215302 (2006).
[6] Contemporaneous thermal measurement on turbulence: D. I. Bradley *et al.*, Nature Phys. **7**, 473 (2011).
[7] See Supplemental Material at http://link.aps.org/supplemental/10.1103/PhysRevLett.107.135302 for a derivation of the heat release.
[8] V. B. Eltsov *et al.*, J. Low Temp. Phys. **161**, 474 (2010).
[9] A. P. Finne *et al.*, Rep. Prog. Phys. **69**, 3157 (2006).
[10] R. Blaauwgeers *et al.*, Phys. Rev. Lett. **89**, 155301 (2002).
[11] V. B. Eltsov *et al.*, in *Prog. Low Temp. Phys.* edited by M. Tsubota (Elsevier B.V., Amsterdam, 2009), Vol. XVI; Prog. Low Temp. Phys. **16**, 45 (2009).
[12] S. N. Fisher *et al.*, Phys. Rev. Lett. **69**, 1073 (1992).
[13] V. B. Eltsov *et al.*, Phys. Rev. Lett. **105**, 125301 (2010).
[14] R. M. Ostermeyer and W. I. Glaberson, J. Low Temp. Phys. **21**, 191 (1975).
[15] A. Calogeracos and G. E. Volovik, Pis'ma Zh. Eksp. Teor. Fiz. **69**, 257 (1999) [JETP Lett. **69**, 281 (1999)].
[16] M. A. Silaev and G. E. Volovik, J. Low Temp. Phys. **161**, 460 (2010).
[17] Yu. M. Bunkov *et al.*, arXiv:1002.1674.